SIMULATION AND ANALYSIS OF THE SOLIDIFICATION CHARACTERISTICS OF A Si-Mo DUCTILE IRON

**G.A. Çelik [a*], M.-I.T. Tzini [b], Ş. Polat [a], J.S. Aristeidakis [b], Ş.H. Atapek [a],
P. I. Sarafoglou [b], G.N. Haidemenopoulos [b,c]**

[a] Kocaeli University, Department of Metallurgical and Materials Engineering, Turkey
[b] University of Thessaly, Department of Mechanical Engineering, Laboratory of Materials, Greece
[c] Khalifa University of Science and Technology, Department of Mechanical Engineering, UAE

Abstract

High silicon and molybdenum ductile cast irons (Si-Mo alloys) are commonly used as exhaust manifold materials suffering from high temperature-oxidation and thermal-mechanical fatigue. The structural integrity of cast Si-Mo alloys under these service conditions is attributed to their microstructure consisting of spheroidal graphite and Mo-rich carbide embedded in a ferritic matrix. However, the cast structure includes also pearlite structure having a detrimental effect on the mechanical properties, therefore the cast matrix needs to be heat treated. In this study, the solidification of a Si-Mo ductile iron was investigated using (i) thermodynamic and kinetic calculations by Thermo-Calc and DICTRA software and (ii) thermal analysis in order to reveal out the sequence of phase formation and the phase transformations during solidification and (iii) microanalysis by energy dispersive spectrometer in order to determine elemental segregation and compare with the calculated values. The solidified structure was also characterized and all microstructural features were specified.

Keywords: Si-Mo cast iron; Thermo-Calc; Solidification; Microstructural characterization

1. Introduction

Today's environmental protection and fuel economy regulations push the manufacturers to design the engines in order to increase power density with reduced emission and improved fuel economy. Increased power density causes higher operating temperatures from the engine to the exhaust system consisting of well-known components, i.e. manifold, catalytic converters, flexible bellow, muffler, resonator, connecting pipes, flanges, and tailpipe [1-5]. Among these components, the manifold is exposed to the highest temperature and subjected to higher thermal and thermomechanical loads due to increased power density [6]. Therefore, it is necessary to design exhaust manifold with appropriate material which provides good high temperature strength, resistance to high temperature corrosion, resistance to microstructural changes, stable physical properties at higher temperatures, thermal shock resistance, and resistance to thermomechanical fatigue [6 - 8]. Although there is an increasing trend in designing new austenitic iron-based alloys [1, 9], high silicon and molybdenum ductile cast iron (SiMo), with ferritic matrix, is one of the strongest candidate

materials due to its low cost and good castability besides its high oxidation resistance and high-temperature strength [10]. The microstructure of Si-Mo alloys consists of spherical graphite and Mo-rich carbide embedded in a ferritic matrix [6, 10]. Ekström et al. indicate that SiMo has lower expansion coefficient, higher thermal conductivity and higher strength than austenitic cast alloys by means of its ferritic matrix [6, 11]. In the matrix design of SiMo cast iron, the amount of Si and Mo plays an important role on the properties of cast alloy, used preferably as high temperature material. The addition of silicon not only enhances the mechanical properties but also improves the oxidation resistance of ductile cast irons due to the formation of complex Si-Fe-O based films, inhibiting further oxygen diffusion into the substrate at elevated temperature [7, 12, 13]. Molybdenum increases the strength and hardness of cast irons by suppressing the pearlite transformation kinetics and it also increases elevated temperature strength and creep resistance [4, 7, 11].

Currently, there is a trend to add alloying elements, i.e. Al, Ni, Cr etc., in order to vary the critical temperatures. This may be very effective in enhancing the properties at elevated temperatures [6,

8, 12, 14-16]. Although there are several studies reporting mechanical [6, 12, 14] and corrosion properties [4, 8, 15], microstructural features [6, 10] of SiMo cast iron as well as microstructural properties of ductile cast irons [17, 18], research on microsegregation, stability of phases and partition of elements in the phases of SiMo ductile cast iron is very limited. It is important to understand (i) the effect of alloying elements on solidification and final microstructure, (ii) macro/microsegregation, (iii) stability of phases, and (iv) partitioning of elements in the phases during solidification in order to improve the Si-Mo ductile cast iron to be used as manifold material by means of controlled microstructure.

Therefore, the objective of this research is to investigate the effect of alloying elements on solidified microstructure of SiMo cast iron and give insight to the spatial distribution of the precipitated phases. For this purpose, the effects of elements were calculated by using the CALPHAD (CALculation of PHAse Diagrams) approach and the microstructure was investigated experimentally in order to compare the calculations with the experimental results.

2. Methodology
2.1. Computational method

Thermo-Calc software which is based on the CALPHAD approach can perform the necessary thermodynamic calculations for various phases in any system [19-21]. For the Fe-C-Si-Mo system under consideration, the thermodynamic database, TCFE6, for ferrous alloys was used. According to several reports, during the solidification the liquid phase transforms into a structure consisting of globular graphite (GR), austenite (γ) and Mo-rich M_6C type carbide [10,11]. With further cooling below the temperature at which ferrite starts to form (T_F), until the room temperature, austenite will eventually transform into ferrite (α) and cementite. The aforementioned phases were considered during the calculations. The simulations were carried out in two stages. The 1st stage comprises the solidification path from $T_{Liquidis}$ (T_L) to $T_{Solidus}$ (T_S) as well as the microsegregation of elements and phases at the end of solidification at T_S using the Scheil module. An important assumption of the Scheil simulation is the absence of diffusion in the solid phases. The results from the 1st stage are then implemented as intial conditions into the 2nd stage, which involves cooling from $T_{Solidus}$ (T_S) to room temperature (T_R) with a cooling rate of 30 °C.min^{-1}.

On the 2nd stage, the phase transformations and the elemental microsegregations were simulated by the computational kinetics software DICTRA, using the MOBFE2 mobility database for ferrous alloys. The DICTRA homogenization model for 1D multiphase

diffusional simulations was employed using a hollow spherical geometry, where the center of the cell corresponds to zero (Fig.1). The distance of the inner interface from the center of cell was taken equal to 10 μm and corresponds to the radius of globular graphite based on the experimental results of the current cast iron used in this study. It was assumed that austenite nucleates and grows along the globular graphite interface, therefore the distance between the inner and outer interface of the spherical cell corresponds to the radius of austenite phase, and was taken equal to 50 μm based on the experimental results. Due to the fact that graphite in the DICTRA software is considered as a diffusion none phase, a typical moving boundary problem approach cannot be adopted in this study. For this reason, an approach for carburization models [22] was applied, in which the boundary conditions set on the inner interface of the cell are

$$a_c = 1 \tag{1}$$

$$\left.\frac{\partial c_k}{\partial x}\right|_{x=10\,\mu m} = 0, k \neq C \tag{2}$$

where a_c is the activity of carbon, and $\partial c_k/\partial x$ is the concentration gradient of element k (mol/m^4). The system is considered closed for all the elements except carbon, since the fluxes J_k (mol/m^{2}s) are equal to zero. The fluxes can be described by Fick-Onsager law for a multicomponent system with n elements,

$$J_k = \sum\nolimits_{(j=1)}^{(n-1)} D_{kj}^n \frac{\partial c_j}{\partial x} \tag{3}$$

where D_{kj}^n is the diffusion coefficient matrix (m^2/s). For the outer interface, the system is considered closed for all elements and the boundary conditions are

$$\left.\frac{\partial c_k}{\partial x}\right|_{x=60\,\mu m} = 0 \tag{4}$$

M_6C carbide, ferrite (α) and cementite were considered as dispersed phases in austenite matrix phase (γ). It should be noted that for the current cast iron used in this study, the flux of carbon in the inner interface can also take negative values, which means that graphite can act as a point sink of carbon in the system. In addition, graphite volume fraction was not included to the total volume of the system since it was regarded as a boundary condition.

Throughout the simulations (i) diffusion was assumed to take place only in the matrix phase, (ii) the dispersed phases acted as point sinks or sources of solute atoms in the simulation and (iii) local equilibrium conditions were imposed at all interfaces. The Hashin–Shtrikman bounds model with prescibed matrix was selected for the description of the

homogenization function of the dispersed phases, which is suitable when diffusion data are known [23].
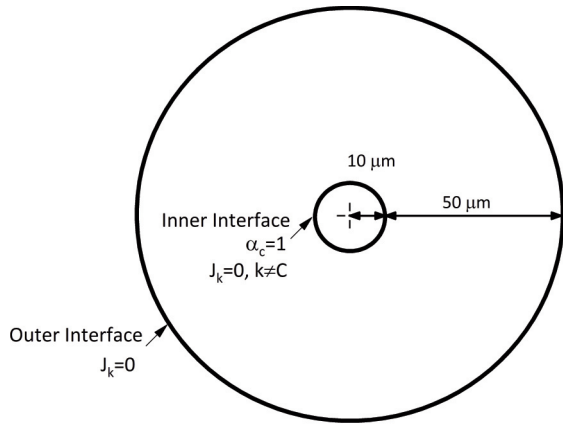
***Figure 1.** Schematic illustration of the cell used in microsegregation calculations*

2.2. Experimental procedure

The studied high silicon and molybdenum ductile cast iron (SiMo) was produced as Y block by sand mold casting according to DIN EN 1563:2012-03 standard at Gedik Casting Co., Turkey. The chemical composition of the SiMo cast iron is given in Table 1. In order to validate the computational results in terms of (i) the formation of the phases during solidification, (ii) critical temperatures of the studied alloy and (iii) microsegregation of the elements, both microstructural examinations and thermal analysis were applied to the SiMo cast iron.

For microscopic examinations, as cast SiMo

***Table 1.** Chemical composition of the SiMo alloy (wt. %)*

C	Si	Mo	Mn	Ni	Fe
3.4	3.6	0.8	0.15	0.05	Bal.

samples were prepared by metallographic method; (i) grinding was carried out with 320, 600, and 1000 mesh size SiC abrasives, respectively, and then the ground surfaces were polished with 3 μm diamond solution, (ii) etching was done with nital (% 3 HNO_3) to reveal out the phases. Microstructural characterization was carried out using a light microscope (LM, Olympus BX41M-LED), scanning electron microscope (SEM, Jeol JSM 6060) and energy dispersive spectrometer (EDS, IXRF). The determined phases by LM were quantified by image analyzer (IA, Olympus BX41M-LED). Thermal analysis was carried out by using Differential Thermal Analyzer (DTA, Netzsch STA 409 PG Luxx). The DTA samples were heated to 1460 °C at a heating rate of 5 °C.min-1, held at that temperature for 5 min, and then cooled to room temperature (T_R) at a rate of 5 °C.min^{-1}.

3. Results and discussion
3.1. Solidification sequence and phase transformations

Phase equilibria and Scheil solidification sequence for the given composition were calculated in order to identify critical temperatures and major phases in the solidified structure. For this purpose, the C isopleth and solidification path were constructed for the SiMo composition (Figure 2). The critical temperatures
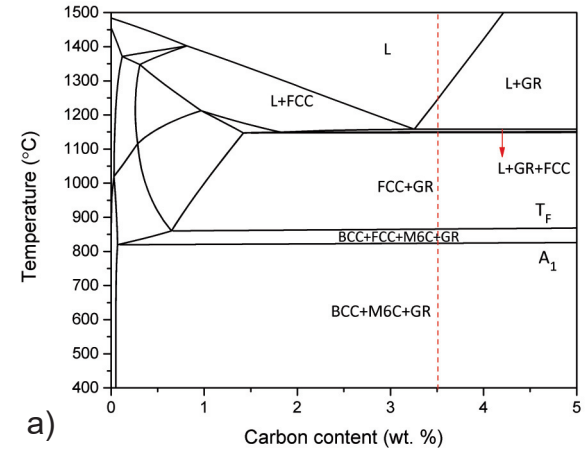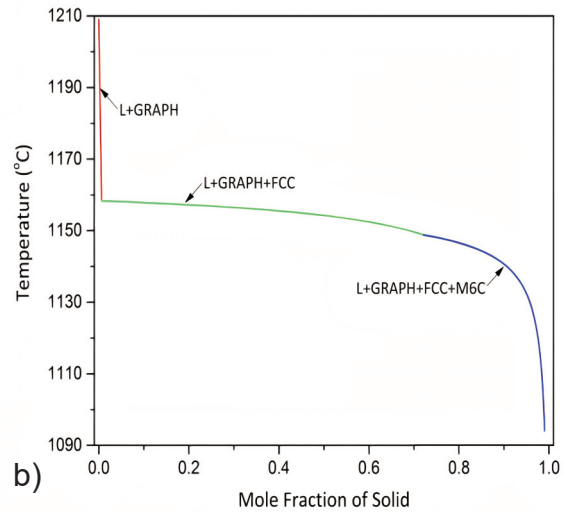
***Figure 2.** Isopleth section (a) and Scheil solidification path (b) of the studied SiMo composition*

were also computed according to equilibrium and values are listed in Table 2. For the solidification sequence, the simulation starts from the liquid phase at casting temperature (T_C=1500 ºC). The solidification path indicates that the solidification

***Table 2.** Critical temperatures (°C) obtained from Thermo-Calc software for the studied alloy*

A_1	T_F	T_C	T_L	T_S	T_R
823.91	865.41	1500	1209	1094	25

begins at liquidus temperature (T_L=1209 ºC) and ends at solidus temperature (T_S=1094 ºC). The sequence of solid phase formation during solidification is L → L + GR (graphite) → L + GR + FCC (austenite) → L + GR + FCC + M_6C (Fig. 2b). After solidification, FCC phase transforms to BCC phase between T_F (865.41 °C) and A_1 (823.91 °C) temperatures (Fig. 2a).

In order to experimentally validate the calculated results, thermal analysis was applied to the SiMo cast iron. The thermogram obtained from DTA analysis is given in Figure 3. The thermogram indicates the
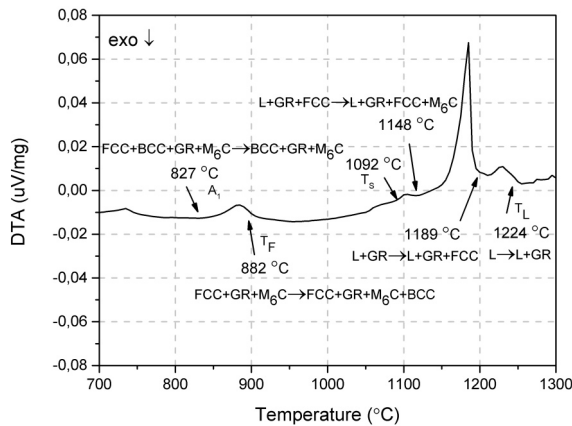

Figure 3. Thermogram indicating the sequence of phase transformations in SiMo alloy

sequence of phase transformations in the studied alloy during cooling from 1460 °C to room temperature. The solidification starts at 1224 °C (T_L) and ends at about 1092 °C (T_S). These values are in agreement with Thermo-Calc data given in Table 2. In this solidification range, graphite precipitates at between 1224 °C and 1189 °C, austenite phase transforms at between 1189 °C and 1148 °C and finally M_6C carbide precipitates at between 1148 °C and 1092 °C. In accordance with the Thermo-Calc data, graphite, austenite, and carbide nucleate from the liquid phase. The transformation of austenite to ferrite starts at 882 °C (T_F) and ends at 827 °C (A_1). The peak at about 730-740 °C corresponds to the magnetic Curie transition of ferrite [24]. According to calculation results given in Figure 2 and the thermogram (Fig. 3), the matrix is expected to consist of ferrite, graphite,

M_6C carbides, and cementite.

In order to clarify the microstructure, LM (Fig. 4a) and SEM (Fig. 4b and c) micrographs showing the cast structure of SiMo alloy are given. As indicated in the micrographs, the cast microstructure of SiMo consists of globular graphite (GR), eutectic carbide (EC), granular cementite (GC) and ferritic matrix as suggested by the calculations (Fig. 2) and thermal analysis (Fig. 3). EDS results obtained from eutectic carbide in Figure 4c indicates that this eutectic carbide is Mo-rich M_6C carbide. According to the image analysis, SiMo cast iron has 11.31 % graphite, 4.23 % carbide and 12.68 % granular cementite in a ferritic matrix. Studies show that this microstructure is a typical microstructure of SiMo cast iron [6, 10].

3.2. Evolution of microsegregation and phase fraction

Microsegregation of elements and phases was calculated in two stages as stated above. The simulation region is a unit spherical cell, where the inner grain boundary corresponds to 10 μm, and the outer grain boundary corresponds to the end of the cell at 60 μm (Fig. 1). In the 1st stage, the microsegregation of the elements in austenite, as well as the fractions of M_6C carbide were computed at the end of the solidification at T_S with the Scheil module of Thermo-Calc. The mole fraction of M_6C carbide in the austenite is depicted in Figure 5. The mole fraction of graphite

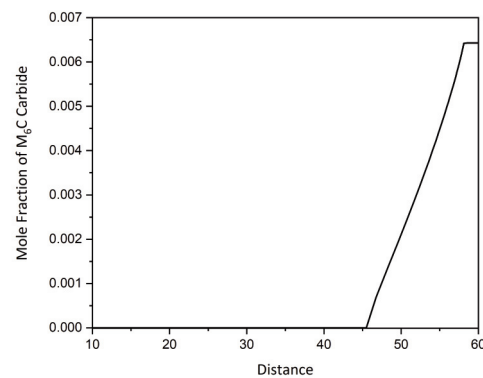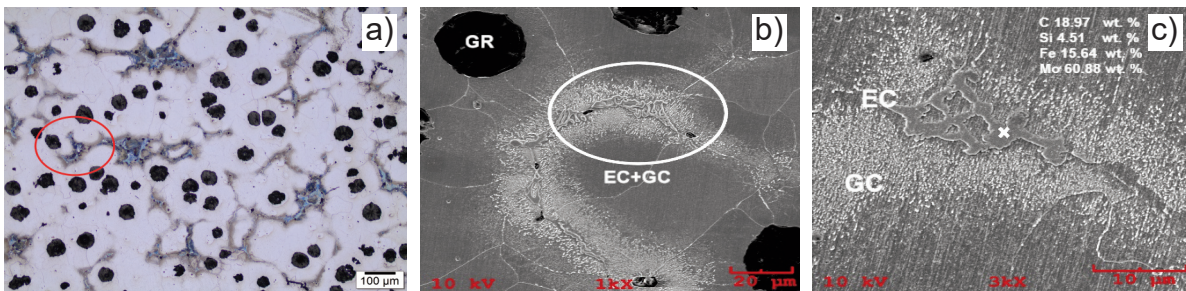*Figure 5. Mole fraction of M_6C carbide in austenite at the end of the 1st stage at T_S*

Figure 4. (a) LM and (b, c) SEM micrographs showing the cast structure of SiMo cast iron

according to Scheil calculations takes a value around 0.082, which approximates the image analysis results. M_6C carbide precipitates only near the boundary, due to carbon segregation. According to solidification studies in the literature, graphite forms from liquid and intercepts the austenite grains [19, 20] while M_6C carbide precipitates at the boundaries due to the microsegregation of the elements [10].

The presence of elemental microsegregation in austenite phase can be calculated at the end of the solidification by Scheil module. Figure 6 shows the compositional profiles for the elements C, Si, Mo, Mn, Ni, and Fe. It can be observed that Si and Ni exhibit negative segregation, whereas the composition
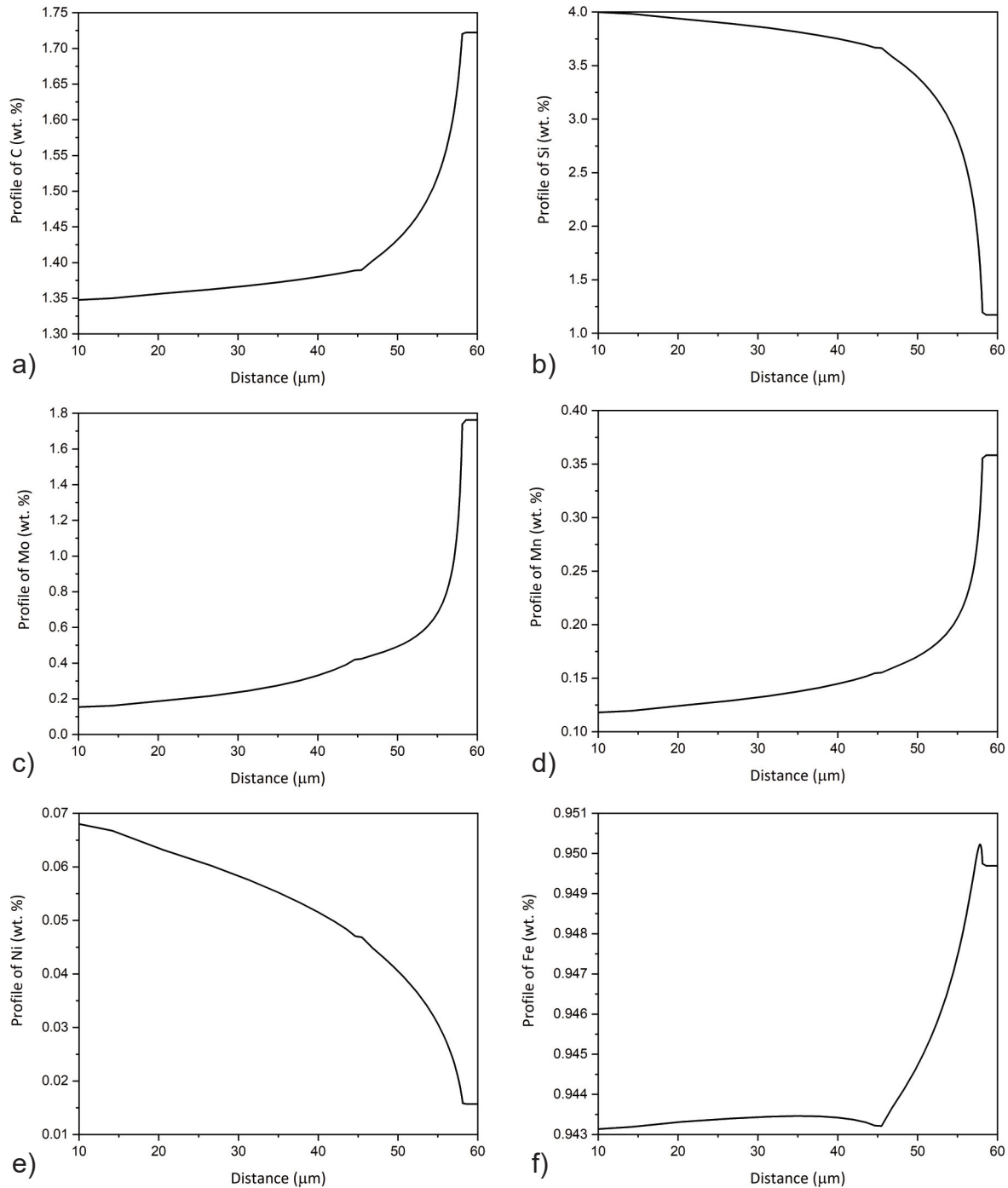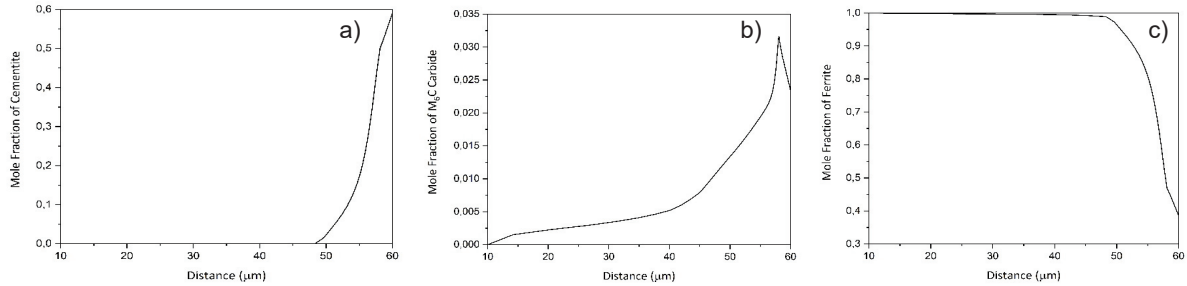

Figure 6. *Composition profiles of (a) C, (b) Si, (c) Mo, (d) Mn, (e) Ni, and (f) Fe in the austenite phase at the end of the 1st stage at T_S*

of the other elements (C, Mo, Mn, Fe) increased towards the grain boundary. In the concentration profiles, a knee at the curve exists at about 45 μm away from the grain center where M_6C begins to form, thus an increase of the mole fraction of C, Mo, and Mn and a decrease of Si and Ni, enables the formation of M_6C close to the grain boundary [13].

Such a formation is also indicated by Figure 5. These findings are in good agreement with the microstructural feature given in Figure 4a, since globular graphite is observed around the middle of the solidified phase, whereas M_6C appears at the grain boundaries.
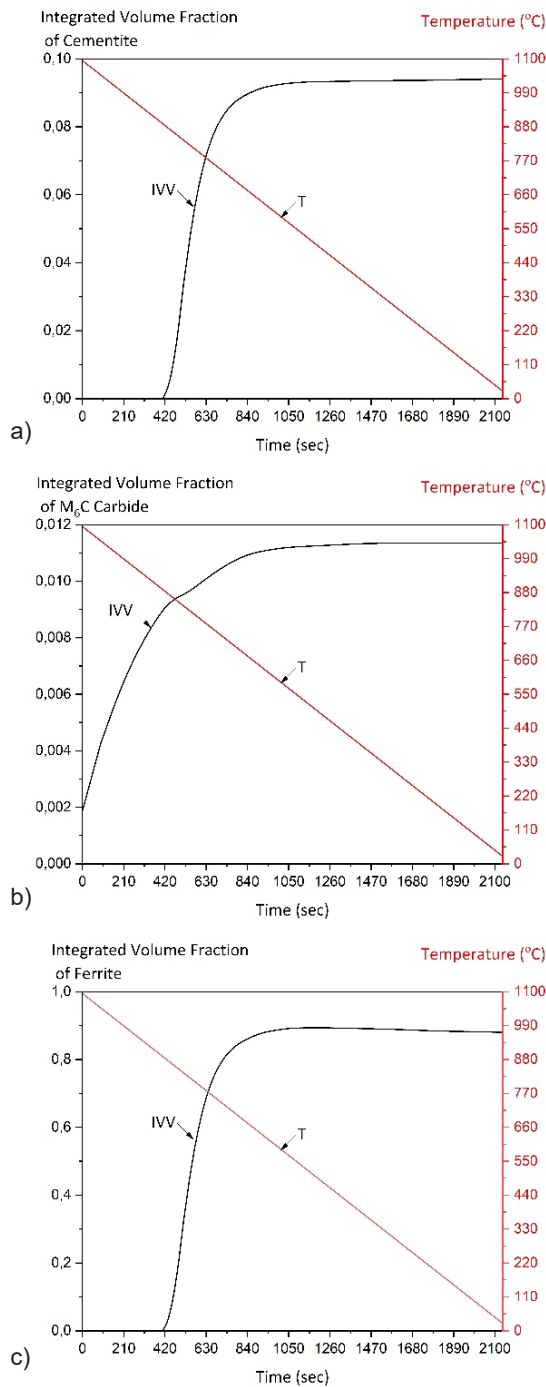
The evolution of the segregation profiles after

Figure 7. *Mole fractions of (a) cementite, (b) M_6C carbide and (c) ferrite phases at the end of the 2nd stage, corresponding to room temperature T_R*
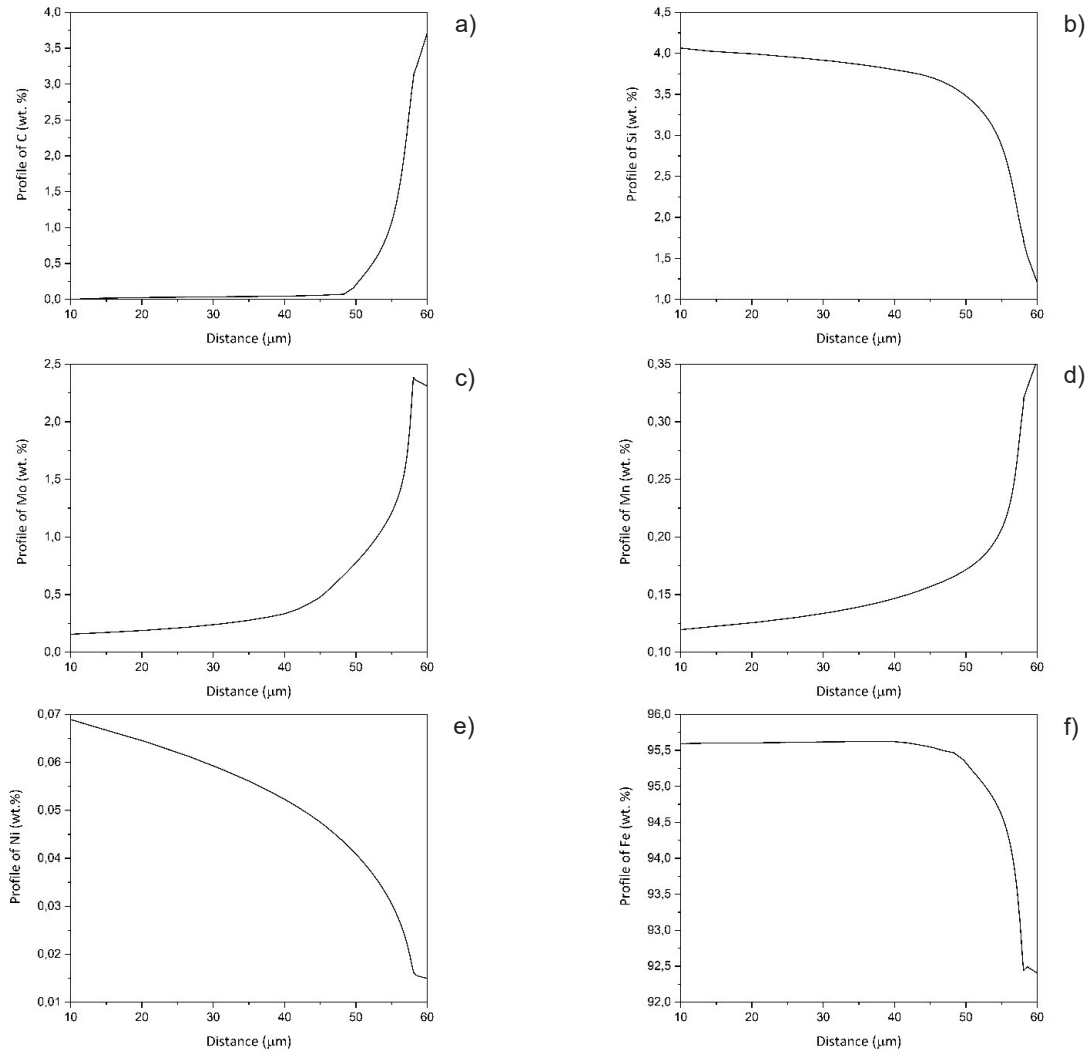
Figure 8. *Composition profiles of (a) C, (b) Si, (c) Mo, (d) Mn, (e) Ni, and (f) Fe at the end of the 2nd stage, corresponding to room temperature T_R*

Figure 9. *Integrated volume fractions of (a) cementite, (b) M_6C carbide and (c) ferrite phases during the 2nd stage*

solidification was simulated with DICTRA software. In the 2nd stage, the composition profiles of C, Si Mo, Mn, Ni, and Fe in austenite phase and the mole fraction of M_6C carbide calculated by Scheil module were used as initial compositions in the austenite matrix phase of the homogenization problem in DICTRA. In this stage, besides M_6C carbide

dispersed phase and graphite which was considered indirectly through the boundary condition, the formation of the dispersed cementite phase and ferrite were expected after cooling to T_R temperature.

The mole fractions of cementite, M_6C carbide, and ferrite formed at end of the 2nd stage, corresponding to T_R temperature are depicted in Figure 7a, 7b and 7c, respectively. The results indicate that cementite and M_6C carbide have precipitated at the grain boundaries. The composition profiles of the simulated region obtained at T_R are given in Figure 8. Although all elements show similar segregation profile at T_R as at T_S, their values are different along the cell structure. While at T_S, due to austenite matrix, carbon composition profile attains values from 1,35 to 1,75 wt. %, at T_R the level of C has decreased at the beginning and the middle of the cell due to the lower solubility of ferrite, and attains a large value around 4 wt. % due to the formation of cementite and M_6C carbide at the grain boundaries. The profiles show that while Mn concentration tends to increase from the inner to outer interface, an opposite behavior is observed for Si. This tendency can be attributed to the occupation of Mn atoms within cementite crystals while Si atoms do not enter the cementite lattice [17]. A clear difference is also observed for the Mo concentration in Figure 6c and 8c. Mo value at the ferrite region is lower than austenite region, since cementite precipitation causes Mo depletion at the ferrite and enrichment at the grain boundaries. Due to the decreased solubility of solute atoms in ferrite, Fe concentration decreases from the inner to outer interface. Despite the differences in composition profiles of the elements at T_R and at T_S, the Ni concentration remains almost unchangeable.

The above calculations on the evolution of microsegregation profiles of the elements reveal out cementite precipitation. The amount of each phase can be represented by the integrated volume fraction (IVV), which can be calculated by DICTRA. The variation IVV of the phases obtained in the 2nd stage are plotted against simulation time in Figure 9. The cooling curve is superimposed in the diagrams and T corresponds to the temperature. Figure 9a shows that cementite precipitates concurrently with the formation of ferrite due to the microsegregation resulting from solidification. Also the absence of graphite as a dispersed phase can explain the earlier formation of cementite. At the end of the simulation time, the volume fractions of cementite and M_6C carbide increase, while the volume fraction of ferrite slightly decreases.

3.3. Validation of calculations by quantitative analysis

In this section, initially a methodology is described briefly and then multi EDS analyses results

in the solidified structure are given, in order to validate the calculations on microsegregation for the 2nd stage mentioned in Section 3.2.

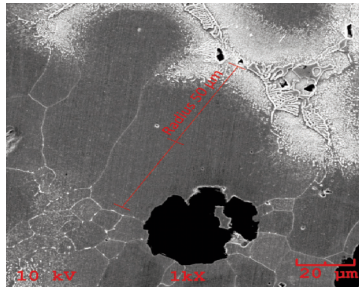A general view is obtained by SEM using topographic contrast as shown in Figure 10, the

Figure 10. *SEM image used for EDS analysis*

diameter of grain structure is marked by a line and 50 μm radius is shown. The EDS analyses were carried out in a large number of grains, from globular graphite until grain boundaries, in order to get statistically reliable results.

The EDS profiles of elements are plotted as a function of distance (Fig. 11). The calculated profiles at the end of the 2nd stage (Fig.8) and the experimentally determined profiles (Fig.11) show similar trends for the alloying elements. Both figures show the negative segregation of Si and Ni and the positive segregation of the other elements. Some numerical differences in weight percentages of the elements between calculated and measured values are due to (a) uncertainties of the experimental parameters used in EDS, (b) due to the fact that Scheil
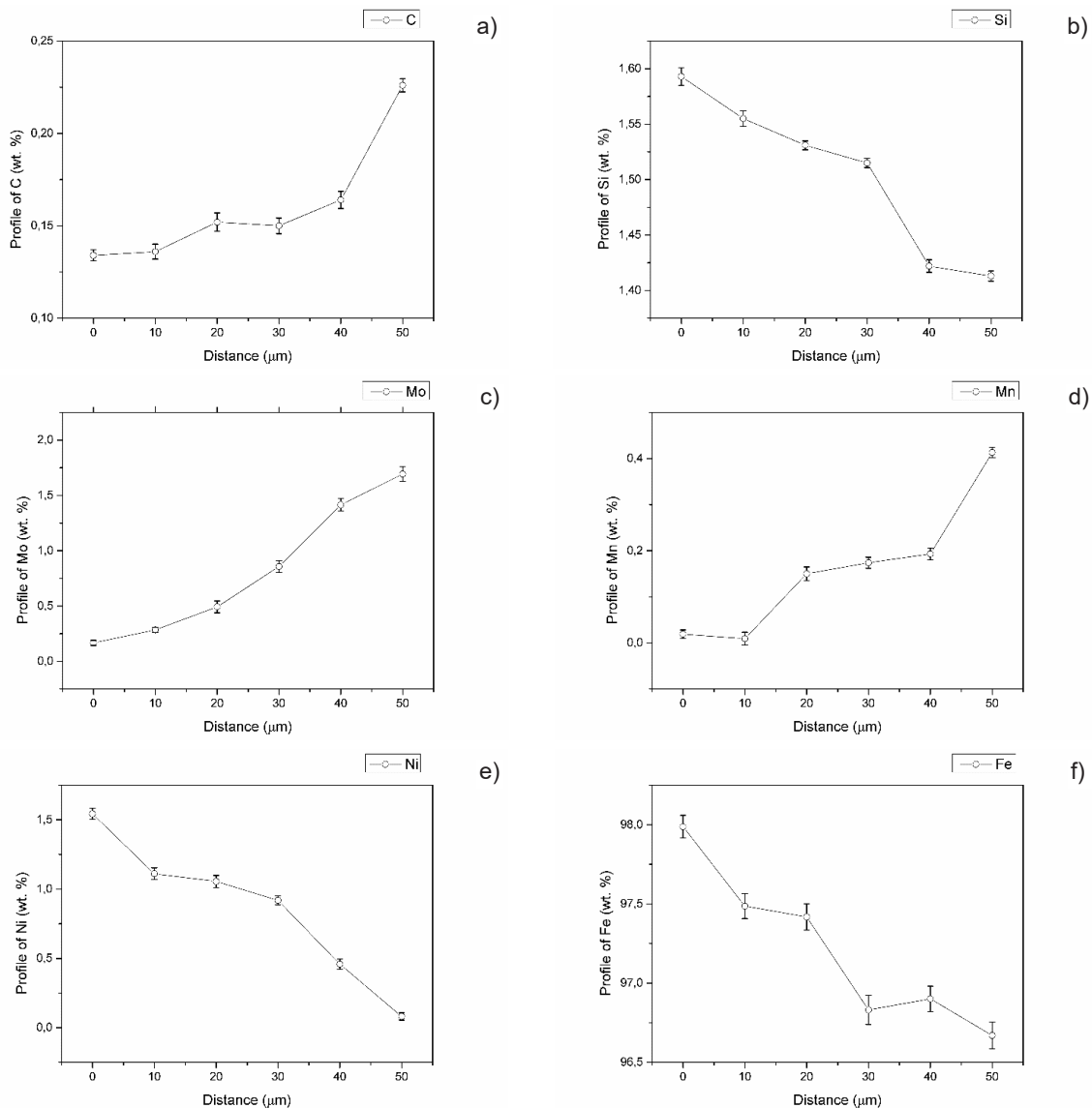

Figure 11. *EDS results of (a) C, (b) Si, (c) Mo, (d) Mn, (e) Ni and (f) Fe at the end of the 2nd stage, corresponding to T_R*

assumptions used for the calculations did not necessarily hold true during the solidification of the samples, and (c) the employed hollow spherical geometry for the 1D diffusional simulations did not reproduce accurately the experimentally observed geometries in the 3D space, as obtained by the SEM micrographs. However, in both qualitative and quantitative terms, there is a good agreement between the calculated composition profiles and the experimental results.

4. Conclusion

In this study, both solidification characteristics and microstructural features of SiMo cast iron as one of the strongest candidate materials for exhaust manifolds were studied by using the CALPHAD approach and metallurgical analyses on cast alloy. Calculations revealed the solidification sequence as the formation of graphite from liquid followed by austenite and M_6C carbide. After solidification, the austenite phase transformed to ferrite phase at about 824 °C, which limits its use at higher temperature. All predicted phases were determined within the ferritic cast structure where graphite and Mo-rich M_6C carbides exist at intercellular regions. Critical temperatures were determined experimentally by DTA and findings supported the calculated results.

In order to follow the microsegregation of the elements, Scheil module of Thermo-Calc was used and the results showed that Si and Ni exhibited negative segregation, whereas the composition of the other elements (C, Mo, Mn) increased towards the grain boundary. Such a finding is useful since it suggests ways to limit the detrimental effect of pearlite by additional alloying elements like aluminium without any further heat treatment. Despite some small numerical differences in weight percentages of the elements, experimental results showed similar trends with the calculated profiles.

A more detailed investigation using a 2D-3D model, such as phase-field or cellular automata models, could yield to some supplementary results and overcome the emerged difficulties ,especially with the graphite phase. Yet, more input data would be required and it would be more computationally demanding. Neverthless, the two stage process simulation, which included the Scheil model and the 1D homogenization model of DICTRA, gave some qualitative and quantitative information inline with the experimental results.

Acknowledgement

References

[1] Y.H. Zhang, M. Li, L.A. Godlewski, J.W. Zindel, Q. Feng, Mater. Sci. Eng. A, 683 (2017) 195-206.

[2] J.P. Shingledecker, P.J. Maziasz, N.D. Evans, M.J. Pollard, Int. J. Press. Vessels Pip., 84 (2007) 21-28.

[3] H-J. Kühn, B. Rehmer, and B. Skrotzki, Int. J. Fatigue, 99 (2017) 295-302.

[4] K. Dawi, J. Favergeon, G. Moulin, Mater. Sci. Forum, 595-598 (2008) 743-751.

[5] M. Ekström, Thibblin A., Tjernberg A., C. Blomqvist, S. Jonsson, Surf. Coat. Technol., 272 (2015) 198-212.

[6] M. Ekström, S. Jonsson, Mater. Sci. Eng. A, 616 (2014) 78-87.

[7] H. Kazdal Zeytin, C. Kubilay, H. Aydın, A.A. Ebrinc, B. Aydemir, J. Iron. Steel Res. Int., 16 (2009) 32-36.

[8] M.P. Brady, G. Muralidharan, D.N. Leonard, J.A. Haynes, R.G. Weldon, R.D. England, Oxid. Met., 82 (2014) 359-381.

[9] K.A. Unocic, S. Dryepondt, Y. Yamamoto, P.J. Maziasz, Metall. Mater. Trans. A, 47(4) (2016) 1641-1653.

[10] L.M. Aberg, C. Hartung, Trans. Indian Inst. Met., 65(6) 2012 633-636.

[11] S. Delprete, Mater. Des., 57 (2014) 528-537.

[12] Y.L. Yang, Z.Y. Cao, Z.S. Lian, H.X. Yu, J. Iron. Steel Res. Int., International, 20 (2013) 52-57.

[13] M.M. Ibrahim, A. Nofal, M.M. Mourad, Metall. Mater. Trans. B, 48 (2017) 1149-1157.

[14] P. Matteis, G. Scavino, A. Castello, D. Firrao, Procedia Mater. Sci., 3 (2014) 2154-2159.

[15] Y.L. Yang, Z.Y. Cao, Y. Qi, B. Liu, Adv. Mater. Res., 97(101) (2010) 530-533.

[16] G.S. Cho, K.H. Choe, K.W. Lee, A. Ikenaga, J. Mater. Sci. Technol., 23 (2007) 97-101.

[17] A. Alhussein, M. Risbet, A. Bastien, J.P. Chobaut, D. Balloy, J. Favergeon, Mater. Sci. Eng., A, 605 (2014) 222-228.

[18] J. Lacaze, Acta Mater., 47(14) (1999) 3779-3792.

[19] ThermoCalc Software System, Foundation of Computational Thermodynamics, Copyright © 1995-2013 Foundation of Computational Thermodynamic, Stockholm, Sweden, (2006).

[20] G.N.Haidemenopoulos, doi 10.13140/RG.2.1.3004.0163, unpublished research.

[21] J.S. Aristeidakis, G.N. Haidemenopoulos, Metall. Mater. Trans. A, 48(5) (2017) 2584-2602.

[22] G.F. Samaras, G.N. Haidemenopoulos, Eng. Fail. Anal. 51 (2015) 29-36.

[23] H. Larsson, L. Höglund, CALPHAD: Computer Coupling of Phase Diagrams and Thermochemistry, 33 (2009) 495-50.

[24] R. Gonzáles-Martinez, U. Torre, J. Lacaze, and J. Sertucha, Mater. Sci. Eng. A, 712 (2018) 794-802.

SIMULACIJA I ANALIZA OSOBINA OČVRŠĆAVANJA Si-Mo DUKTILNOG GVOŽĐA

G.A. Çelik [a*], M.-I.T. Tzini [b], Ş. Polat [a], J.S. Aristeidakis [b], Ş.H. Atapek [a], P. I. Sarafoglou [b], G.N. Haidemenopoulos [b,c]

[a] Univerzitet Kodžaeli, Odsek za metalurgiju i inženjerstvo materijala, Turska
[b] Univerzitet u Tesaliji, Odsek za mašinstvo, Laboratorija za materijale, Grčka
[c] Kalifa univerzitet nauke i tehnologije, Odsek za mašinstvo, Ujedinjeni Arapski Emirati

Apstrakt

Duktilno liveno gvožđe sa visokim sadržajem silicijuma i molibdena (Si-Mo legure) se uobičajeno koristi kao materijal za izduvne kolektore koji trpe oksidaciju usled visoke temperature i termomehanički zamor. Strukturni integritet livenih Si-Mo legura pod ovim uslovima rada pripisuje se njihovoj mikrostrukturi koja se sastoji od sferoidnog grafita i karbida bogatog molibdenom u feritnoj matrici. Pa ipak, livena struktura takođe uključuje i perlitnu strukturu koja ima štetan uticaj na mehaničke osobine, i zato je potrebno da livena matrica bude termički obrađena. U ovom istraživanju očvršćavanje Si-Mo duktilnog gvožđa je ispitivano (i) pomoću termodinamičkih i kinetičkih proračuna softverima Thermo-Calc i DICTRA i (ii) termalnom analizom da bi se otkrio redosled nastajanja i transformacije faze tokom očvršćavanja kao i (iii) mikroanalizom pomoću energetskog disperzivnog spektrometra da bi se odredila segregacija elemenata i uporedila sa izračunatim vrednostima. Takođe je opisana očvrsnuta struktura i navedene su sve mikrostrukturne osobine.

Ključne reči: *Si-Mo liveno gvožđe; Thermo-Calc; Očvršćavanje; Mikrostrukturna karakterizacija*